AIAA AVIATION Forum
17-21 June 2019, Dallas, Texas
AIAA Aviation 2019 Forum

10.2514/6.2019-2966

AIAA Aviation Forum and Exposition, 17 - 21 June 2019, Dallas, Texas

Assessment of the Elliptic Blending Reynolds Stress Model for a Rotating Turbulent Pipe Flow Using New DNS Data

Neil Ashton[1]*, Jefferson Davis[2]†, Christoph Brehm[2]‡

[1]*Department of Engineering Science, University of Oxford, UK.*

[2]*Department of Mechanical Engineering, University of Kentucky, Lexington, KY 40506, USA.*

New direct numerical simulation data of a fully-developed axially rotating pipe at $Re = 5300$ and $Re = 19,000$ is used to examine the performance of the second-moment closure elliptic blending Reynolds stress model for a range of rotation rates from N=0 to N=3. In agreement with previous studies (using alternative second-moment closure models), the turbulence suppression observed by the DNS is over-predicted. This over-prediction is greatest at $Re = 5,300$ and most noticeable in the poor prediction of the $\overline{u'w'}$ turbulent shear-stress component. At N=3 the flow is completely relaminarized in contrast to the DNS that is only partly relaminarized. The accuracy of the second-moment closure model is superior to the two-equation $k-\omega$ SST model which predicts pure solid-body rotation, however, both are equally poor at the highest rotation rates. The accuracy of each model is also assessed for the initial portion of a rotating pipe where in contrast to the fully-developed rotating pipe flow the turbulent suppression is under-predicted compared to the DNS. It is clear that greater work is required to understand the root cause of the poor prediction by these second-moment closure models and further DNS and experimental work is underway to assist this effort.

I. Introduction

Rotating and swirling flows are fundamental to a wide range of industrial applications, from inside a jet engine to the vortices shed from airplanes and cars. In addition to flow separation and transition, they pose a key challenge to the development of accurate turbulence modelling approaches. As the flow is rotated, the turbulence moves towards an anisotropic state which invalidates the majority of one and two-equation Reynolds-Averaged Navier-Stokes (RANS) approaches and has led to these cases being used to develop and validate second-moment closure methods that account directly for this anisotropy by modelling each Reynolds Stress individually. An example of a geometrically simple, yet rich in physics case is an axially rotating pipe that is the subject of this paper. The axially rotating pipe can be described by two non-dimensional parameters, *i.e.* the Reynolds number $Re = UD/\nu$ based on the mean bulk flow velocity U, the pipe diameter D, and the kinematic viscosity ν as well as the rotation number $N = V_w/U$ of the pipe. The rotation number characterizes the angular velocity Ω through the azimuthal velocity of the pipe inner wall, $V_w = \Omega D/2$.

Numerous experiments have been conducted for an axially rotating pipe, the first being that of White et al.[1] who observed a reduction of up to 40% in the pressure loss (i.e lower skin-friction) for high rotation rates. Kikuyama et al.[2] experimentally observed that an initially turbulent flow can be relaminarized with sufficiently large N while initially laminar flow was found to be destabilized by the rotation. Later Nishibori et al.[3] found similar findings observing the initial section of the rotating pipe saw turbulent suppression towards relaminarization but beyond $x/D = 60$ that turbulent bursts appeared as the flow is destabilized. The experimental setup was however only up to $x/D = 120$ which may not have reached a fully-developed state.[4]

*Senior Researcher, Senior AIAA member
†Ph.D. Student, AIAA member.
‡Assistant Professor, AIAA member.

Given the challenges of experimental studies (due to the long length of pipe required to reach a fully-developed state) and the desire to better understand the turbulent budgets, a number of Direct Numerical Simulation (DNS) studies have been undertaken. These, however, have been conducted at lower Reynolds numbers than the experiments ($Re < 7400$) due to the large computational cost, and have not to date considered a fully-developed stationary pipe flow leading into a rotating section, assuming instead a fully-developed periodic rotating section.

Imao et al.[5] confirmed a reduction of turbulence intensity with increasing rotation rate and verified a relationship between the reduced mixing length and the Richardson number. Orlandi et al.[6] conducted the most extensive DNS, studying rotation numbers up to $N = 2$ at $Re = 4,900$ and later up to $N = 10$ in Orlandi et al.[7] They both observed a relaminarization process where the mean streamwise velocity profile is approaching the laminar Poiseuille profile, while Nishibori et al.[3] and Reich et al.[8] explained the changes in the mean flow and the turbulence by drawing a general connection to the centrifugal force, Orlandi et al.[6] concluded that this occurred through modification of the near wall flow structures.

Given the relevance to more complex flows, a great deal of attention has been placed on the performance of RANS models for this flow. Jakirlic et al.[9] conducted an extensive review of the challenges for RANS models in correctly predicting the flow physics associated with rotating and swirling flows. For the axially rotating pipe (using the DNS data from Orlandi et al.[6]) they concluded that even a low-Reynolds number second-moment closure model (Hanjalic–Jakirlic (HJ) RSM[10]) could not correctly capture the flow beyond N=0.5. At rotation rates greater than N=0.5, they found that the RANS models predicted much lower turbulence levels than the DNS which led to complete relaminarization. This tendency was also observed in a number of previous studies using two-equation and second moment closure models,[11].[12–14] Poroseva et al.[13,15] & Olsen[16] focused on assessing more sophisticated turbulent diffusion models that account for higher-order moment components, Pettersson et al.[14] focused on the near-wall modeling by the use of an elliptic-relaxation based RSM model with Jakirlic et al.[10] assessing a range of pressure-strain models. None of these approaches could capture the correct level of turbulent suppression. One of the uncertainties centres around the value of the $u^{'}w^{'}$ Reynolds stress component. In the experimental work of Imao et al.[17] they observed for $Re = 20,000$ at $x/D = 120$ for N=0, 0.5 & 1 that both $u^{'}v^{'}$ and $u^{'}w^{'}$ decreased with increasing rotation rate but that importantly $u^{'}w^{'}$ was negative and became more negative at higher rotation rates. This is in contrast to the DNS work[7][18] which albeit was conducted at a lower $Re = 5,300$. The majority of these prior RANS simulations predicted a negative $u^{'}w^{'}$ component. Pettersson et al.[14] commented that the correct prediction of $u^{'}w^{'}$ is essential as this indirectly affects the axial velocity due to the $u^{'}w^{'}$ equation.

Whilst much of the previous work has focused on a fully-developed axially rotating pipe flow, Ashton et al.[4] and others[19][16] have also focused on the setup of a fully-developed stationary turbulent pipe flow leading into a rotating pipe section which is more in-line with experimental setups (and flows observed in industrial applications). This setup (which does not have any DNS data to date) is challenging for experiments as a very long pipe ($x/D = 0 - 300$) is required to firstly establish fully-developed stationary flow and then to reach a fully-developed rotating flow. For this reason there is only experimental data available up to $x/D = 120$ at $Re = 10,000$[3] which from the RANS results of Ashton et al.[4] suggests may not be long enough to reach a fully-developed state. An alternative experimental setup is that of Zaets et al.[20] which at a higher $Re = 37,000$ focused on the non-fully developed rotating section by using a pipe of $x/D = 100$ of which the final $x/D = 25$ was rotating. In this setup, there is strong turbulence suppression in both the turbulent shear-stresses and the turbulent normal-stresses even at $N = 0.6$ at $x/D = 25$. This turbulence suppression is captured by the RANS models (both two-equation and second-moment closure) but the strength of the turbulence suppression is under-predicted.[4,16,19] Interestingly, the different turbulence modelling approaches predict a very different fully-developed solution at $x/D = 200$ (for which there is no experimental or DNS data available) where a two-equation model predicts a return to higher turbulence values compared to the stationary pipe i.e turbulent enhancement compared to turbulent suppression for the second-moment closure model.[4] A similar situation was observed in[15] where different second-moment closure formulations gave a wide range of results by $x/D = 200$, also varying between turbulent suppression and turbulent enhancement.

For this reason, a new experimental and numerical campaign has begun by the authors and colleagues under a National Science Foundation grant (awards OCI-0725070 and ACI-1238993) to conduct DNS and experiments of a complete stationary and rotating pipe up to $x/D = 200$. In this work, we discuss the initial DNS data up to $Re = 19,000$ for a fully-developed rotating pipe (see Davis et al.[21] for complete details of these initial results). The complete stationary-to-rotating pipe will be conducted over the coming 12 months and will be subject of future papers.

Current DNS Simulation Setup

The DNS setup is fully explained in Davis et al.,[21] but summarized here for reference. A DNS study of fully-developed rotating turbulent pipe flow was conducted for three Reynolds numbers, Re= 5,300, 11,700, and 19,000. Four rotation rates were considered for each Reynolds number, N= 0, 0.5, 1, and 3, with the non-rotational case (N= 0) being used for verification of the DNS method. For the computational domain shown in Figure 1, a size of L/D= 12.5 was selected, as this was determined by Khoury et al.[22] to be sufficient to ensure that velocities at locations separated by a distance of $O(L)$ are uncorrelated for pipe flows of up to Re= 37700. To ensure sufficient grid resolution to fully capture the wide range of turbulent scales, the grid spacings presented in Table 1 were calculated from skin friction values computed for non-rotating turbulent pipe flow simulations. As turbulence suppression induces a reduction in skin friction, these values were deemed to be conservative estimates for the rotational cases. The grid spacings shown in Table 1 are presented as ranges in y^+-units, as the mesh varies within the computational domain, as seen in Figure 1.

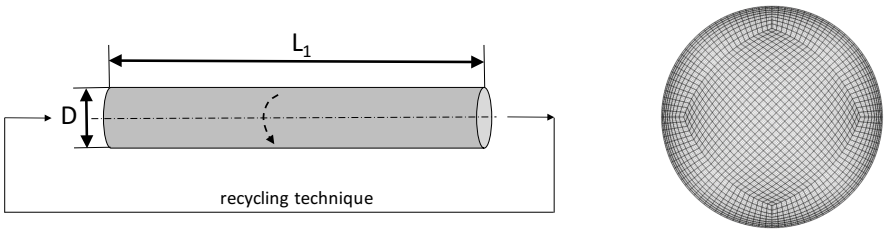

Figure 1. Simulation domain and mesh cross-section for the fully developed turbulent flow simulations.

The timestep, Δt, was chosen to ensure a the CFL condition is satisfied with CFL= 0.75. Averages were calculated over 20, 11.5, and 6.5 flow throughs for Re= 5,300, 11,700, and 19,000, respectively and were conducted after a short initial transient period.

The spectral element based Navier-Stokes solver Nek5000 was selected to perform the DNS of turbulent rotating pipe flows. Nek5000 is a higher-order accurate incompressible solver which uses a weighted-residual approach for spatial discretization. Three parallel algorithms are tested at the beginning of each run, and the optimal algorithm is chosen, ensuring parallelism is tuned automatically for each HPC system.[23] Matrix operations are implemented in assembler code M×M routines to speed up computations, and Nek5000 uses minimal external libraries to increase compile speed.

The mesh is comprised of hexahedral elements with the solution being composed of Nth-order tensor product polynomials within each element. Local lexicographical ordering within each macro element, and the need to evaluate only $\mathcal{O}(EN^4)$ discrete operators, which typically have $\mathcal{O}(EN^6)$ non-zeros, leads to the cache and vectorization efficiency (see Ref. 23).

The full DNS dataset will be the subject of a future publication and made publicly available once the remaining higher $Re = 37,000$ simulation is completed.

Table 1. Details of turbulent pipe flow simulations assuming a streamwise extend of $15D$, where Re refers to Reynolds number, Δr^+, $\Delta R\Theta^+$ and Δz^+ are the grid spacings measured in y^+-units and $N_{\Delta x}$ is the number of grid points in the computational domain. Note that for the grid spacings different ranges are provided because the mesh is non-uniform.

Re	Δr^+/ $\Delta R\Theta^+$/ Δz^+	$N_{\Delta x} \times 10^6$
5,300	0.14–4.4/1.5–4.5/3.0–9.9	20
11,700	0.16–4.7/1.5–5.0/3.0–9.9	120
19,000	0.15–4.5/1.5–4.8/3.0–10.	440

II. Turbulence Models

The elliptic blending Reynolds-Stress model, the EBRSM-ε_H,[24] is the focus of the current RANS model simulations, however the $k-\omega$ SST model[25] is also assessed to compare to a commonly used two-equation model. What follows is a description of the EBRSM ε_h model,[24] referred to in this paper as the EBRSM

model, followed by the $k-\omega$ SST.

Assuming an incompressible flow; the Reynolds averaged Navier-Stokes equations are given by:

$$\frac{\partial \overline{u}_i}{\partial x_j} = 0 \tag{1}$$

and,

$$\frac{\partial \overline{u}_i}{\partial t} + \overline{u}_j \frac{\partial \overline{u}_i}{\partial x_j} = -\frac{\partial \overline{p}}{\partial x_i} + \nu \frac{\partial^2 \overline{u_i}}{\partial x_j \partial x_j} - \frac{\partial \tau_{ij}}{\partial x_j}, \tag{2}$$

where $\overline{u}_i$ denotes the Reynolds averaged velocity and $\tau_{ij} = \overline{u_i' u_j'}$ denotes the Reynolds stress tensor. The RSMeb model is a modification of the standard Elliptic Blending model by Manceau.[12] The main novelty is given by the use of the homogeneous dissipation rate ε^h as the scale providing equation. The modeled transport equation for the Reynolds stress tensor is given by:

$$\frac{\partial \tau_{ij}}{\partial t} + \overline{u}_j \frac{\partial \tau_{ij}}{\partial x_j} = P_{ij} + \Phi^*_{ij} - \varepsilon^h_{ij} + \frac{\partial}{\partial x_k}\left[\left(0.5\nu\delta_{kl} + C_k \frac{k}{\varepsilon^h}\tau_{kl}\right)\frac{\partial \tau_{ij}}{\partial x_l}\right], \tag{3}$$

where P_{ij} is the production, Φ^*_{ij} is the pressure redistribution term, ε^h_{ij} is the homogeneous dissipation rate tensor[10] and the last term represents molecular diffusion and turbulent transport according to the Daly-Harlow model[26] with $C_k = 0.21$. The homogeneous dissipation rate[10] is used:

$$\varepsilon^h = \varepsilon - 0.5\nu \frac{\partial^2 k}{\partial x_l x_l}, \tag{4}$$

where k is the turbulent kinetic energy $k = \tau_{ll}/2$. The production term is given by:

$$P_{ij} = -\tau_{ik}\frac{\partial \overline{u}_j}{\partial x_k} - \tau_{jk}\frac{\partial \overline{u}_i}{\partial x_k}. \tag{5}$$

In the EB model, the redistribution term is given by a "linear blending" of a near wall model Φ^w_{ij} and a homogeneous model Φ^h_{ij} that is appropriate away from the wall

$$\Phi^*_{ij} = (1-f_\alpha)\Phi^w_{ij} + f_\alpha \Phi^h_{ij}, \tag{6}$$

where $f_\alpha = \alpha^3$ is the blending function which is based on the variable α that defines the "closeness" to a solid wall and that satisfies an elliptic equation:[12]

$$\alpha - L_d^2 \nabla^2 \alpha = 1. \tag{7}$$

The boundary conditions at solid walls are $\alpha = 0$ and in the free stream $\alpha = 1$. The Durbin-limited[27] length scale L_d is given by:

$$L_d = max\left(C_L \frac{k^{3/2}}{\varepsilon^h}, C_\eta \frac{\nu^{3/4}}{(\varepsilon^h)^{1/4}}\right), \tag{8}$$

with constants $C_L = 0.13$ and $C_\eta = 10$. The dissipation rate tensor is a blend between the near wall anisotropic form and the common isotropic form away from the wall[10,12]

$$\varepsilon^h_{ij} = (1-f_\alpha)\frac{\tau_{ij}}{k}\varepsilon^h + f_\alpha \frac{2}{3}\varepsilon^h \delta_{ij}. \tag{9}$$

The homogeneous part of the redistribution term is modeled according to the SSG model[28]

$$\begin{aligned}\Phi^h_{ij} = &-\left(C_{g1} + C^*_{g1}\frac{P}{\varepsilon^h}\right)\varepsilon^h a_{ij} + C_{g2}\left(a_{ik}a_{kj} - \frac{1}{3}a_{kl}a_{kl}\delta_{ij}\right) + \left(C_{g3} - C^*_{g3}\sqrt{a_{kl}a_{kl}}\right)kS_{ij} \\ &+ C_{g4}k\left(a_{ik}S_{jk} + a_{jk}S_{ik} - \frac{2}{3}a_{lm}S_{lm}\delta_{ij}\right) + C_{g5}k\left(a_{ik}\Omega_{jk} + a_{jk}\Omega_{ik}\right),\end{aligned} \tag{10}$$

where $P = P_{kk}/2$ is the production of turbulent kinetic energy, $a_{ij} = \tau_{ij}/k - 2/3\delta_{ij}$ is the anisotropy tensor, $S_{ij} = 1/2\left(\frac{\partial \overline{u}_i}{\partial x_j} + \frac{\partial \overline{u}_j}{\partial x_i}\right)$ is the rate-of-strain tensor, and $\Omega_{ij} = 1/2\left(\frac{\partial \overline{u}_i}{\partial x_j} - \frac{\partial \overline{u}_j}{\partial x_i}\right)$ is the rate-of-rotation tensor. The model coefficients are $C_{g1} = 1.7$, $C^*_{g1} = 0.9$, $C_{g2} = 1.05$, $C_{g3} = 0.8$, $C^*_{g3} = 0.65$, $C_{g4} = 0.625$, $C_{g5} = 0.2$.

The near wall form of the redistribution model was derived in[29] such that the correct asymptotic behavior is obtained

$$\Phi_{ij}^{w} = -5\frac{\varepsilon^h}{k}\left(\tau_{ik}n_jn_k + \tau_{jk}n_in_k - \frac{1}{2}\tau_{kl}n_kn_l\left(n_in_j + \delta_{ij}\right)\right), \tag{11}$$

where the wall normal vector $\vec{n}$ is also obtained from the elliptic variable α by

$$\vec{n} = \frac{\nabla\alpha}{\|\nabla\alpha\|}. \tag{12}$$

The closure of the dissipation rate equation follows the proposal of Jakirlić and Hanjalić[10] but with a simplified term for the viscous production:

$$\frac{\partial\varepsilon^h}{\partial t} + \overline{u}_j\frac{\partial\varepsilon^h}{\partial x_j} = C_{\varepsilon 1}P\frac{\varepsilon^h}{k} - C_{\varepsilon 2}f_\varepsilon\frac{\tilde{\varepsilon}^h\varepsilon^h}{k} + E_\varepsilon + \frac{\partial}{\partial x_k}\left[\left(0.5\nu\delta_{kl} + C_\varepsilon\frac{k}{\varepsilon^h}\tau_{kl}\right)\frac{\partial\varepsilon^h}{\partial x_l}\right], \tag{13}$$

with

$$E_\varepsilon = 2C_{\varepsilon 3}\nu\frac{k^2}{\varepsilon^h}\left(1-\alpha\right)\left(\frac{\partial^2\overline{u}_i}{\partial x_k\partial x_k}\right)^2, \tag{14}$$

and

$$\tilde{\varepsilon}^h = \varepsilon^h - \nu\left(\frac{\partial\sqrt{k}}{\partial n}\right)^2. \tag{15}$$

The function f_ε is modified from a Re_t dependent formulation[10] to be a function of the elliptic near wall variable α and is given by

$$f_\varepsilon = 1 - \frac{C_{\varepsilon 2} - C_{\varepsilon 1}}{C_{\varepsilon 2}}\exp\left[-\left(7\alpha\right)^5\right]. \tag{16}$$

The model coefficients are given by:

$$C_{\varepsilon 1} = 1.44,\ \ C_{\varepsilon 2} = 1.82,\ \ C_{\varepsilon 3} = 0.005,\ \ C_\varepsilon = 0.18. \tag{17}$$

The boundary conditions at the wall are

$$\overline{u}_i = 0,\ \ \tau_{ij} = 0,\ \ \varepsilon^h = \nu\frac{k}{y_1^2},\ \ \alpha = 0, \tag{18}$$

where y_1 is the wall normal distance of the first cell center.

The turbulent viscosity is calculated by

$$\nu_t = C_\mu\frac{k^2}{\varepsilon^h}\det\left(\frac{\tau_{ij}}{k}\right), \tag{19}$$

with $C_\mu = 0.28$.

The recent review paper of Manceau et al.[12] provides more details on the origin of the model and the various versions that have been developed since its inception. The implementation of this model in OpenFOAM was verified in Stoellinger et al.[24] for a number of test-cases. The $k-\omega$ SST model is used as an example of the performance of a commonly used two-equation model in industry. We use the following form of the model:

$$\frac{Dk}{Dt} = \min(P_k, 20\ C_\mu\ k\omega) - C_\mu k\omega + \frac{\partial}{\partial x_j}\left[\left(\nu + \nu_t\sigma_k\right)\frac{\partial k}{\partial x_j}\right] \tag{20}$$

$$\frac{D\omega}{Dt} = \alpha\frac{P_k}{\nu_t} - \beta\omega^2 + \frac{\partial}{\partial x_j}\left[\left(\nu + \frac{\nu_t}{\sigma_\omega}\right)\frac{\partial\omega}{\partial x_j}\right] + 2(1-F_1)\frac{\sigma_{\omega 2}}{\omega}\frac{\partial k}{\partial x_j}\frac{\partial\omega}{\partial x_j} \tag{21}$$

$$P_k = \nu_t S^2 \tag{22}$$

$$S = \sqrt{2S_{ij}S_{ij}} \tag{23}$$

Where the turbulent viscosity is computed from:

$$\nu_t = \frac{a_1 k}{\max(a_1\omega, SF_2)}\ ,\ a_1 = 0.31 \tag{24}$$

$$F_2 = \tanh(\arg_2^2) \tag{25}$$

$$\arg_2 = \max\left(\frac{2\sqrt{k}}{C_\mu \omega y}, \frac{500\nu}{y^2\omega}\right) \tag{26}$$

The function F_1 that combines the model constants and blends the $k-\varepsilon$ and $k-\omega$ models is defined as:

$$F_1 = \tanh(\arg_1^4) \tag{27}$$

$$\arg_1 = \min\left[\max\left(\frac{\sqrt{k}}{C_\mu \omega y}, \frac{500\nu}{y^2\omega}\right), \frac{4\rho k}{\sigma_{\omega 2} CD_{k\omega} y^2}\right] \tag{28}$$

$$CD_{k\omega} = \max\left(2\sigma_{\omega 2}\frac{1}{\omega}\frac{\partial k}{\partial x_j}\frac{\partial \omega}{\partial x_j}, 10^{-20}\right) \tag{29}$$

Where y is the distance to the nearest wall.

The values of the model constants α, β, σ_k and σ_ω from Equations 20 & 21 are combined using the blending function F_1. Which for α is:

$$\alpha = F_1\alpha_1 + (1-F_1)\alpha_2 \tag{30}$$

$$\beta = F_1\beta_1 + (1-F_1)\beta_2 \tag{31}$$

Where α_1 corresponds to the value of α in the $k-\omega$ mode and α_2 corresponds to the value of α in the $k-\varepsilon$ mode. Table 2 shows the model constants for both modes.

	$k-\omega$ mode (1)	$k-\varepsilon$ mode (2)
σ_k	0.85	1.0
σ_ω	0.5	0.856
β	0.0750	0.0828
C_μ	0.09	
κ	0.41	
$\alpha = \beta/C_\mu - \sigma_\omega\kappa^2/\sqrt{C_\mu}$		
α	0.553	0.440

Table 2. Model coefficients for the $k-\omega$ SST model

All simulations were conducted in OpenFOAM using an incompressible steady-state solver based upon the SIMPLE pressure-velocity coupling method (simpleFoam). Second order accurate upwind schemes (linearUpwind) were used for spatial discretization for both the momentum and turbulent quantities. As shown in Ashton et al.[4] mesh convergence is reached on modest grids and for this study 128 cells are used in the radial direction with a $y^+ < 1$ along the length of the pipe. Periodic boundary conditions are used for the inlet/outlet boundaries where the pressure-gradient is adjusted to impose the correct Reynolds number.

III. Results

Figures 2, 3 and 4 show the axial and azimuthal velocity components and the turbulent quantities for the EBRSM at a Reynolds number of 19000 for a fully-developed axially rotating pipe flow for several rotation rates (N=0, 0.5, 1.0 & 3.0). The axial velocity shows the same trend as the DNS data to move towards a laminar profile as the rotation rate increases, however beyond N=0.5, the EBRSM moves towards a completely laminar profile in contrast to a more gradual shift for the DNS. This is due to the under-prediction of the turbulent shear-stress component $\overline{u'v'}$ that is the main contributor to the axial velocity.

The results shown here agree with the trends observed in previous results of Jakirlic et al.,[9] Peterson et al.[14] and Poroseva et al.[13] The previous authors did not consider the higher rotation rate of N=3 but at this rotation rate, the turbulent shear-stresses have gone to zero, which is also reflected in the zero values for the normal Reynolds stresses i.e complete relaminarization. Interestingly unlike some of the previous work using RSM models for this case,[9,14] the $u^{'}w^{'}$ shear stress component is over-predicted but has a positive sign which is in contrast to others who computed this to be negative. It is the subject of continuing work to look into the turbulent budgets and undertake a term-by-term analysis to understand this differing behaviour. Nevertheless this shear-stress component is still the least well predicted of all the turbulence component at N=0.5 and beyond and is still likely to be responsible for the poor prediction of the model for this case.

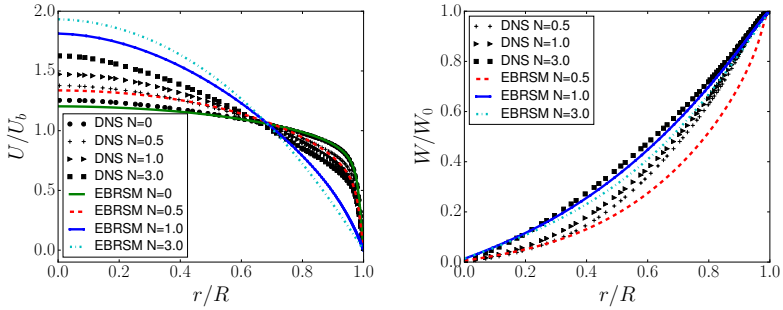

Figure 2. Fully-Developed Rotating Pipe (N=0,0.5,1.0,3.0): (Left to Right), Axial Velocity (U/U_b), Azimuthal velocity W/W_0 for the EBRSM, compared to the current DNS data at Re=19,000

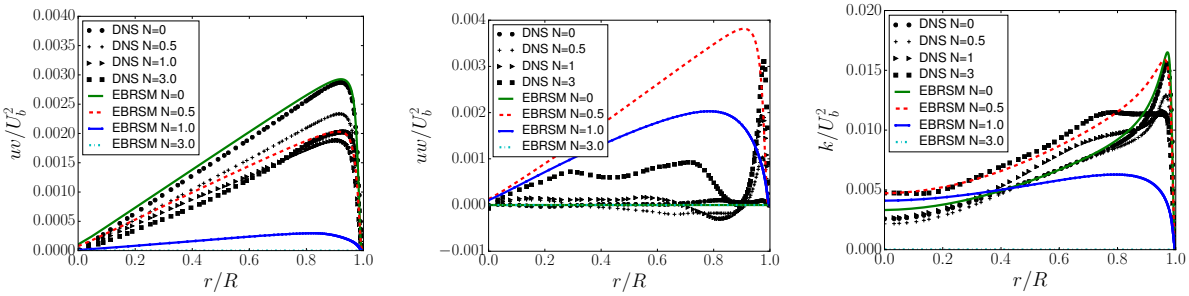

Figure 3. Fully-Developed Rotating Pipe (N=0,0.5,1.0,3.0): (Left to Right), Reynolds Stress ($u^{'}v^{'}/U_b^2$), ($u^{'}w^{'}/U_b^2$) and Turbulent Kinetic Energy (k/U_b^2) for the EBRSM, compared to the current DNS data at Re=19,000

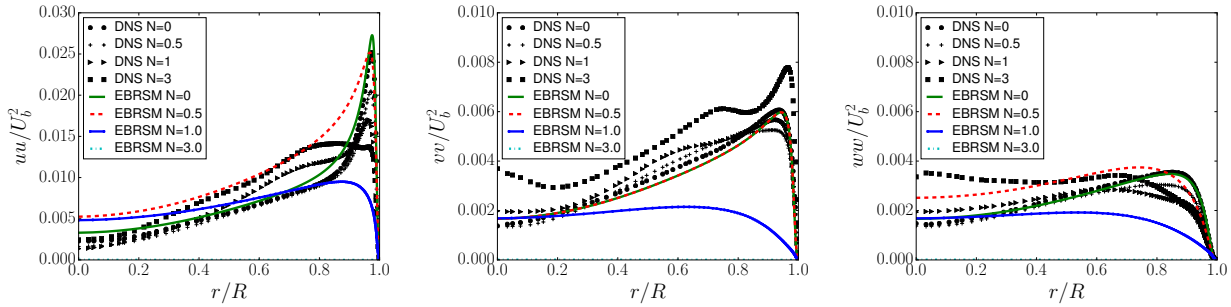

Figure 4. Fully-Developed Rotating Pipe (N=0,0.5,1.0,3.0): (Left to Right), Reynolds Stress ($u^{'}u^{'}/U_b^2$),($v^{'}v^{'}/U_b^2$) & ($w^{'}w^{'}/U_b^2$) EBRSM, compared to the current DNS data at Re=19,000

Figures 5, 6 and 7 show the axial and azimuthal velocity components and the turbulent quantities for the $k-\omega$ SST model. It can be seen that in agreement with Wallin et al.[30] that the two-equation model (without any additional non-linear terms) is unable to predict anything other than a linear profile i.e solid-body rotation regardless of the rotation rate. This is due to the fact that a linear azimuthal profile means zero $u^{'}w^{'}$ component and therefore no contribution of the shear-stress to the azimuthal velocity. In contrast to the EBRSM model (and other RSM results) the $k-\omega$ SST shows a constant reduction in turbulence levels as opposed to the RSM models which initially predict higher normal stresses between N=0 & N=0.5.

Also, whereas the EBRSM predicts complete relaminarization by N=3 (and a corresponding laminar axial velocity profile) the $k-\omega$ SST model still shows turbulence and therefore the axial velocity is closer to the DNS data.

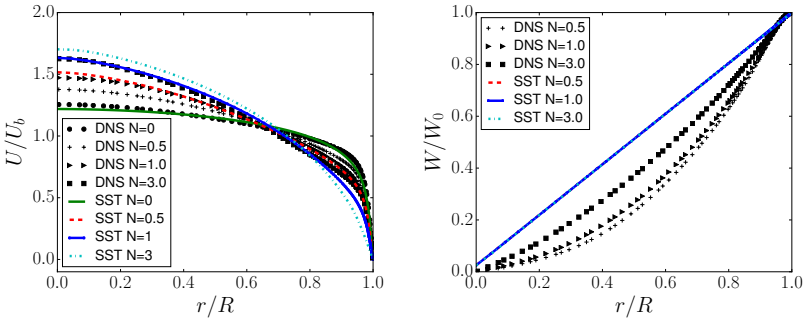

Figure 5. Fully-Developed Rotating Pipe (N=0,0.5,1.0,3.0): (Left to Right), Axial Velocity (U/U_b), Azimuthal velocity W/W_0 for the SST, compared to the current DNS data at Re=19,000

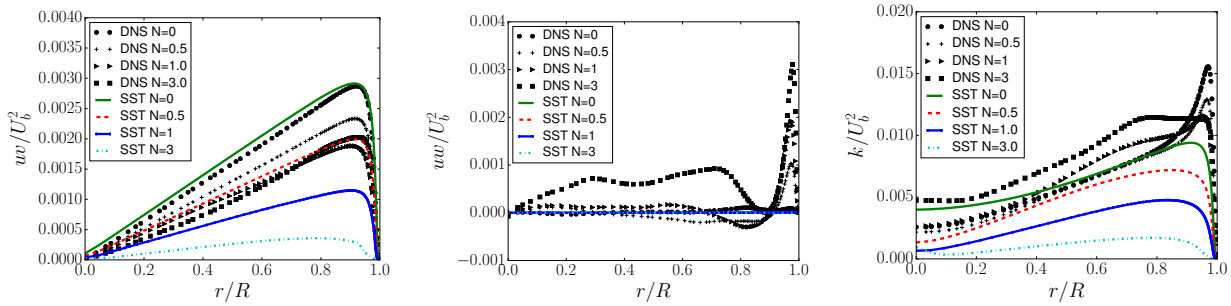

Figure 6. Fully-Developed Rotating Pipe (N=0,0.5,1.0,3.0): (Left to Right), Reynolds Stresses ($u^{'}v^{'}/U_b^2$),($u^{'}w^{'}/U_b^2$) and Turbulent Kinetic Energy (k/U_b^2) for the SST, compared to the current DNS data at Re=19,000

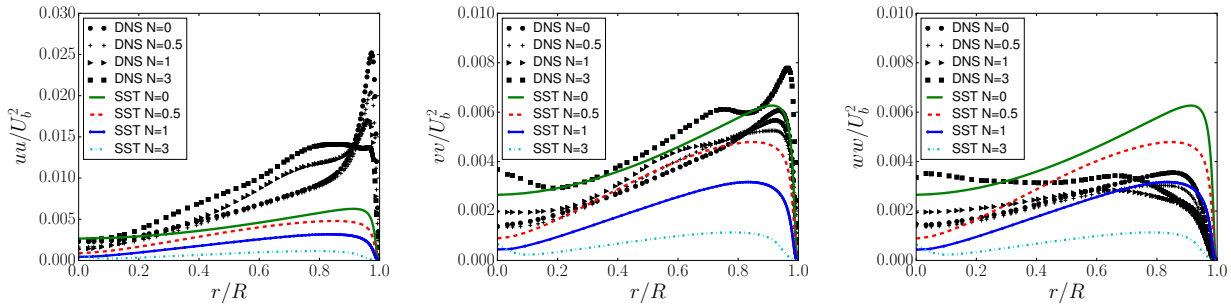

Figure 7. Fully-Developed Rotating Pipe (N=0,0.5,1.0,3.0): (Left to Right), Reynolds Stresses ($u^{'}u^{'}/U_b^2$),($v^{'}v^{'}/U_b^2$) & ($w^{'}w^{'}/U_b^2$) SST, compared to the current DNS data at Re=19,000

Figures 8, 9 and 10 show the axial and azimuthal velocity components and the turbulent quantities at the lower $Re = 5300$, which corresponds to the previous DNS of Orlandi et al.[7] It can be seen that compared to $Re = 19,000$ the EBRSM shows even earlier relaminarization with the azimuthal velocity showing a fully laminar profile even at N=1. This again agrees with Jakirlic et al.,[9] Peterson et al.[14] and Poroseva et al.[13] Given the different flavours of RSM models in terms of pressure-strain, turbulent diffusion and the dissipation rate equation suggests a more general inability for these models to capture the underlying flow physics. An interesting observation is that the sign of $u^{'}w^{'}$ differs at N=0.5 and N=1 for $Re = 5,300$ and $Re = 19,000$ and therefore may explain partially why there was disagreement between the DNS of Orlandi et al.[7] and Eggels et al.[18] which were conducted at $Re = 5,300$ and the experiments which were conducted at $Re = 20,000$.

As discussed previously an additional challenge that was studied in Ashton et al.[4] is the setup studied experimentally by Zaets et al.,[20] i.e. a fully-developed stationary pipe flow leading into an axially rotating

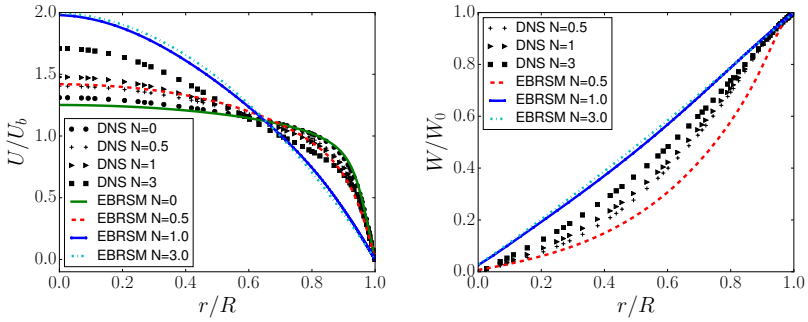

Figure 8. Fully-Developed Rotating Pipe (N=0,0.5,1.0,3.0): (Left to Right), Axial Velocity (U/U_b), Azimuthal velocity W/W_0 for the EBRSM, compared to the current DNS data at Re=5,300

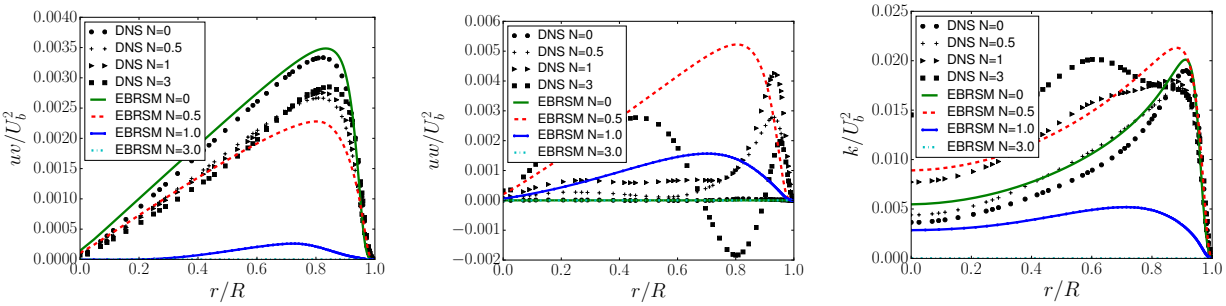

Figure 9. Fully-Developed Rotating Pipe (N=0,0.5,1.0,3.0): (Left to Right), Reynolds Stress ($u'v'/U_b^2$), ($u'w'/U_b^2$) and Turbulent Kinetic Energy (k/U_b^2) for the EBRSM, compared to the current DNS data at Re=5,300

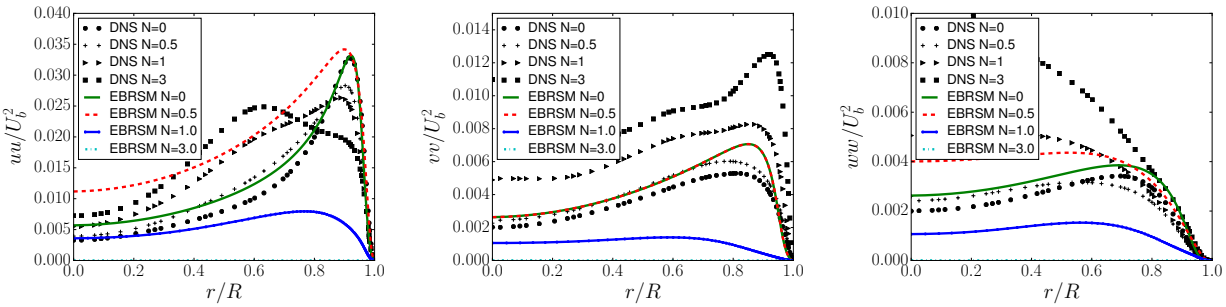

Figure 10. Fully-Developed Rotating Pipe (N=0,0.5,1.0,3.0): (Left to Right), Reynolds Stress ($u'u'/U_b^2$),($v'v'/U_b^2$) & ($w'w'/U_b^2$) EBRSM, compared to the current DNS data at Re=5,300

pipe of length $X/D = 200$. Figures 11 and 12 show the profiles of the axial and azimuthal velocities together with the shear-stress and turbulent kinetic energy at $x/D = 25$ into the rotating section for N=0.6 and $Re = 37,000$. It can be seen that turbulent suppression is present in the experimental data and this is under-predicted by both the EBRSM and SST models. This is shown more clearly in Figure 13 for the ratio of the normal Reynolds stresses in the stationary pipe to rotating pipe at $x/D = 25$. It can be seen that indeed all the stresses are not damped as strongly as the experimental data. This is in contrast to Figure 4 for the fully-developed pipe flow where at N=0.5 (at a lower $Re = 19,000$) the CFD predicts too much suppression of the turbulent stresses. Finally, the most interesting difference between the experiment and both RANS approaches is shown in Figure 14 for the damping coefficient along the axial direction at $r/R = 0$. It shows that the EBRSM model predicts initially turbulence suppression but then enhancement once the flow reaches an almost fully-developed state at $x/D = 200$ whereas the $k-\omega$ SST shows turbulence suppression for the whole pipe. Unfortunately, the experimental data is only available until $x/D = 25$ and so at present we cannot validate the CFD findings. This condition will be studied over the coming year using DNS and later experimentally by the authors and colleagues to better understand the flow physics and the accuracy of different RANS approaches.

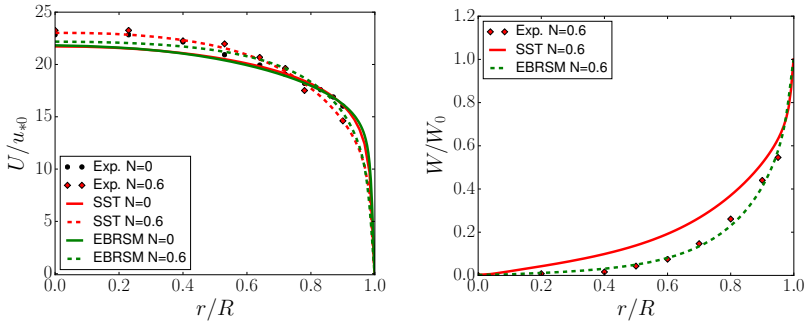

Figure 11. Rotating Pipe (N=0.6): (Left to Right), Axial Velocity (U/u_{*0}), Azimuthal velocity W/W_0 for the SST and EBRSM, compared to experimental data of Zaets et al.[20]

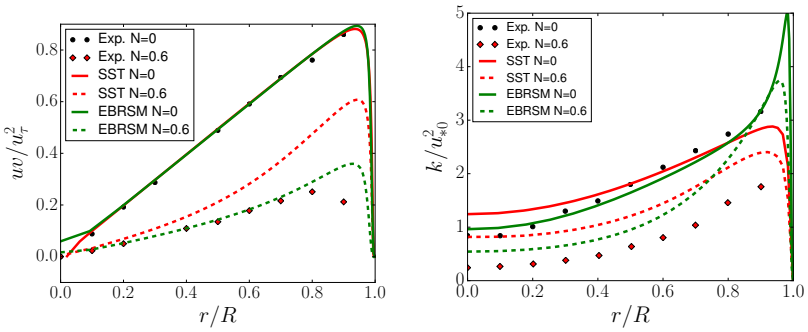

Figure 12. Rotating Pipe (N=0.6): (Left to Right), Reynolds Stress ($u^{'}v^{'}/u_{*0}^2$)and Turbulent Kinetic Energy (k/u_{*0}^2) for the SST and EBRSM, compared to experimental data of Zaets et al.[20]

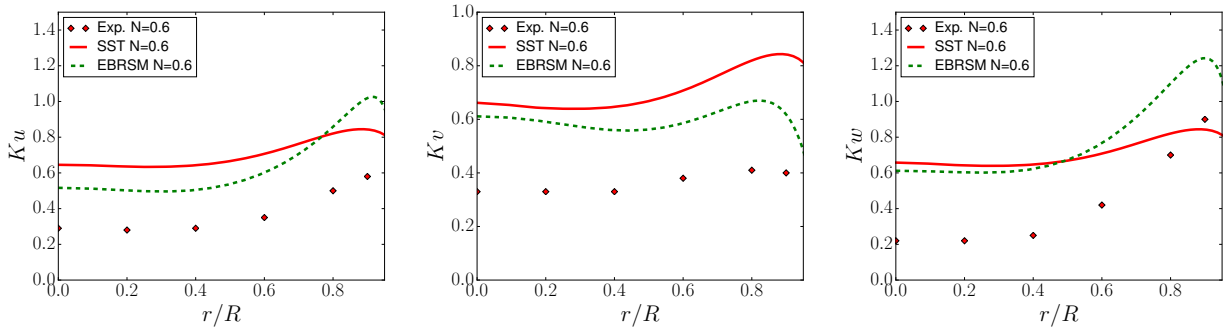

Figure 13. Rotating Pipe (N=0.6): (Left to Right), Damping coefficient $Ku =< u^{'}u^{'} > (N > 0)/ < u^{'}u^{'} > (N = 0)$ at $x/D = 25$, Damping coefficient $Kv =< v^{'}v^{'} > (N > 0)/ < v^{'}v^{'} > (N = 0)$ at $x/D = 25$ and Damping coefficient $Kw =< w^{'}w^{'} > (N > 0)/ < w^{'}w^{'} > (N = 0)$ at $x/D = 25$ for the SST and EBRSM, compared to experimental data of Zaets et al.[20]

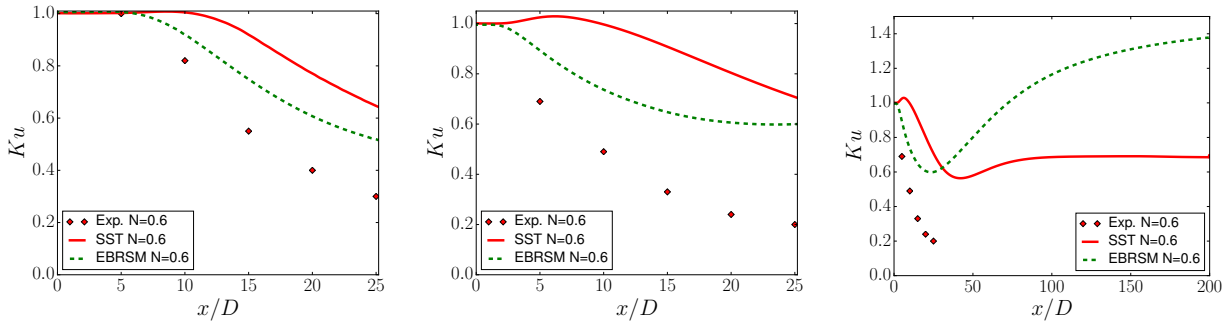

Figure 14. Rotating Pipe (N=0.6): (Left to Right), Damping coefficient Ku at $r/R = 0$, Damping coefficient Ku at $r/R = 0.6$ and Damping coefficient Ku at $r/R = 0.6$ (whole pipe length) for the SST and EBRSM, compared to experimental data of Zaets et al.[20]

IV. Conclusions and outlook

The flow through an axially rotating pipe has been studied using new direct numerical simulation data at $Re = 5,300$ & $Re = 19,000$ for rotation rates N = 0,0.5,1, and 3 to assess the predictive capability of the second-moment closure elliptic blending Reynolds-stress model (EBRSM). It was found that in agreement with previous studies using second-moment closure models that the level of turbulence suppression is over-predicted compared to the new DNS at $Re = 5,300$ and $Re = 19,000$. For N=3, the EBRSM model predicts complete relaminarization with zero turbulence in contrast to the DNS data. The $u^{'}w^{'}$ turbulent shear-stress component is identified as being the greatest challenge for the EBRSM which is worse at $Re = 5,300$. The two-equation $k-\omega$ SST model is unable to predict the correct azimuthal velocity instead predicting solid-body rotation regardless of the rotation rate. The accuracy of each model is also assessed for the initial portion of a rotating pipe where in contrast to the fully-developed rotating pipe flow the turbulent suppression is under-predicted compared to the DNS. There is, however, limited experimental data and no DNS to compare and understand the flow physics towards the final fully-developed state. Further work is required to undertake a term-by-term analysis using the new DNS data to gain additional insight into the source of the modelling errors and suggest alternative formulations.

Acknowledgments

The authors would like to acknowledge the use of the University of Oxford Advanced Research Computing (ARC) facility in carrying out this work. Special thanks to Michael Olsen (NASA Ames Research Center), Chris Rumsey (NASA Langley Research Center) and Professor Svetlana Poroseva (University of New Mexico) for their helpful discussions on this work. Particular thanks goes to Professor Michael Stoellinger (University of Wyoming) for prior work on the EBRSM-ϵ_h model and this test-case. JD and CB gratefully acknowledge funding from the National Science Foundation under award CBET-1706346 with Dr. R.Joslin as Program Manager. Part of his research is part of the Blue Waters sustained-petascale computing project, which is supported by the National Science Foundation (awards OCI-0725070 and ACI-1238993) and the state of Illinois. Blue Waters is a joint effort of the University of Illinois at Urbana-Champaign and its National Center for Supercomputing Applications. This work used the Extreme Science and Engineering Discovery Environment (XSEDE), which is supported by National Science Foundation grant number ACI-1548562. Research was conducted using the Stampede2 and Comet HPC systems through allocation TG-CTS180008.

References

[1]White, A., "Flow of a fluid in an axially rotating pipe," *Journal of Mechanical Engineering Science*, Vol. 6, No. 1, 1964, pp. 47–52.

[2]Kikuyama, K., Murakami, M., Nishibori, K., and Maeda, K., "Flow in an Axially Rotating Pipe: A calculation of flow in the saturated region," *Bull. JSME*, Vol. 26, No. 214, 1983, pp. 506–513.

[3]Nishibori, K., Kikuyama, K., and Murakami, M., "Laminarization of turbulent flow in the inlet region of an axially rotating pipe." *JSME international journal*, Vol. 30, No. 260, 1987, pp. 255–262.

[4]Ashton, N. and Stoellinger, M. K., "Computation of Turbulent Flow in a Rotating Pipe using the Elliptic Blending Reynolds Stress Model," *46th AIAA Fluid Dynamics Conference*, , No. June, 2016, pp. 1–11.

[5]Imao, S., Itoh, M., and Harada, T., "Turbulent characteristics of the flow in an axially rotating pipe," *International Journal of Heat and Fluid Flow*, Vol. 17, No. 5, 1996, pp. 444–451.

[6]Orlandi, P. and Fatica, M., "Direct simulations of turbulent flow in a pipe rotating about its axis," *Journal of Fluid Mechanics*, Vol. 343, 1997, pp. 43–72.

[7]Orlandi, P. and Ebstein, D., "Turbulent budgets in rotating pipes by DNS," *International Journal of Heat and Fluid Flow*, Vol. 21, No. 5, 2000, pp. 499–505.

[8]Reich, G. and Beer, H., "Fluid flow and heat transfer in an axially rotating pipe—I. Effect of rotation on turbulent pipe flow," *International Journal of Heat and Mass Transfer*, Vol. 32, No. 3, 1989, pp. 551–562.

[9]Jakirlic, S., Hanjalic, K., and Tropea, C., "Modeling Rotating and Swirling Turbulent Flows: A Perpetual Challenge," *AIAA Journal*, Vol. 40, No. 10, 2002, pp. 1984–1996.

[10]Jakirlic, S. and Hanjalic, K., "A new approach to modelling near-wall turbulence energy and stress dissipation," *Journal of Fluid Mechanics*, Vol. 539, 2002, pp. 139–166.

[11]Shih, T., Zhu, J., and Liou, W., "Modelling of turbulent swirling flows," Tech. rep., NASA TM 113112, 1997.

[12]Manceau, R., "Recent progress in the development of the Elliptic Blending Reynolds-stress model," *International Journal of Heat and Fluid Flow*, Vol. 51, 2015, pp. 195–220.

[13]Poroseva, B. S. V., Kassinos, S. C., Langer, C. a., and Reynolds, W. C., "Computation of turbulent flow in a rotating pipe using the structure-based model," *Center for Turbulence Research Annual Research Briefs*, 2000, pp. 279–290.

[14]Pettersson, B. A., Andersson, H. I., and Brunvoll, A. S., "Modeling near-wall effects in axially rotating pipe flow by elliptic relaxation," *AIAA Journal*, Vol. 36, No. 7, 2012, pp. 1164–1170.

[15]Kurbatskii, A. F. and Poroseva, S. V., "Modeling turbulent diffusion in a rotating cylindrical pipe flow," *International Journal of Heat and Fluid Flow*, Vol. 20, 1999, pp. 341–348.

[16]Olsen, M. E., "Reynolds-stress and triple-product models applied to flows with rotation and curvature," *46th AIAA Fluid Dynamics Conference*, American Institute of Aeronautics and Astronautics, Reston, Virginia, 6 2016.

[17]Imao, S. and Itoh, M., "Turbulent characteristics of the flow in an axially rotating pipe," *International Journal of Heat and Fluid Flow*, 1996.

[18]Eggels, J., *Direct and Large Eddy Simulation of Turbulent Flow in a Cylindrical Pipe Geometry*, Ph.D. thesis, Delft University, 1994.

[19]Poroseva, S. V., Kassinos, S. C., Langer, C. a., and Reynolds, W. C., "Structure-based turbulence model: Application to a rotating pipe flow," *Physics of Fluids*, Vol. 14, No. 4, 2002, pp. 1523–1532.

[20]Zaets, P. G., Kurbatskii, A. F., Onufriev, A. T., Poroseva, S. V., Safarov, N. A., Safarov, R. A., and Yakovenko, S. N., "Experimental study and mathematical simulation of the characteristics of a turbulent flow in a straight circular pipe rotating about its longitudinal axis," *Journal of Applied Mechanics and Technical Physics*, Vol. 39, No. 2, 3 1998, pp. 249–260.

[21]Davis, J., Sparsh, G., Ashton, N., Bailey, S., and Brehm, C., "A DNS Study to Investigate Turbulence Suppressionin Rotating Pipe Flows," *AIAA Aviation 2019*, 2019.

[22]El Khoury, G. K., Schlatter, P., Noorani, A., Fischer, P. F., Brethouwer, G., and Johansson, A. V., "Direct numerical simulation of turbulent pipe flow at moderately high Reynolds numbers," *Flow, turbulence and combustion*, Vol. 91, No. 3, 2013, pp. 475–495.

[23]Fischer, P., Lottes, J., and Kerkemeier, S., "Nek5000, http://nek5000.mcs.anl.gov," 2008.

[24]Stoellinger, M., Roy, R., and Ashton, N., "Application of an elliptic blending Reynolds stress model in attached and separated flows," *22nd AIAA Computational Fluid Dynamics Conference*, 2015.

[25]Menter, F. R., "Two-Equation Eddy-Viscosity Turbulence Models for Engineering Applications," *AIAA*, Vol. 32, No. 8, 1994, pp. 1598–1605.

[26]Daly, B. J. and Harlow, "Transport equations in turbulence," *Phys. Fluids*, Vol. 13, 1970, pp. 2634–2649.

[27]Durbin, P., "Limiters and wall treatments in applied turbulence modeling," *Fluid Dynamics Research*, Vol. 41, No. 1, 2 2009, pp. 012203.

[28]Speziale, C. G., Sarkar, S., and Gatski, T. B., "Modelling the pressure strain correlation of turbulence: an invariant dynamical systems approach," *Journal of Fluid Mechanics*, Vol. 227, 1991, pp. 245–272.

[29]Manceau, R. and Hanjalic, K., "Elliptic blending model: A new near-wall Reynolds-stress turbulence closure," *Physics of Fluids*, Vol. 14, 2001, pp. 744–754.

[30]Wallin, S. and Johansson, A. V., "An explicit algebraic Reynolds stress model for incompressible and compressible turbulent flows," *Journal of Fluid Mechanics*, Vol. 403, 2000, pp. 89–132.